GDCh

Research Articles

Angewandte
Chemie
International Edition
www.angewandte.org

Porphyrin-Based COF 2D Materials: Variable Modification of Sensing Performances by Post-Metallization

Ming Liu[+], Yong-Jun Chen[+], Xin Huang[+], Long-Zhang Dong, Meng Lu, Can Guo, Daqiang Yuan, Yifa Chen,* Gang Xu,* Shun-Li Li, and Ya-Qian Lan*

Abstract: *2D nanomaterials with flexibly modifiable surfaces are highly sought after for various applications, especially in room-temperature chemiresistive gas sensing. Here, we have prepared a series of COF 2D nanomaterials (porphyrin-based COF nanosheets (NS)) that enabled highly sensitive and specific-sensing of NO_2 at room temperature. Different from the traditional 2D sensing materials, H_2-TPCOF was designed with a largely reduced interlayer interaction and predesigned porphyrin rings as modifiable sites on its surfaces for post-metallization. After post-metallization, the metallized M-TPCOF (M = Co and Cu) showed remarkably improved sensing performances. Among them, Co-TPCOF exhibited highly specific sensing toward NO_2 with one of the highest sensitivities of all reported 2D materials and COF materials, with an ultra-low limit-of-detection of 6.8 ppb and fast response/recovery. This work might shed light on designing and preparing a new type of surface-highly-modifiable 2D material for various chemistry applications.*

[*] C. Guo, Prof. Y. Chen, Prof. S.-L. Li, Prof. Y.-Q. Lan
School of Chemistry, National and Local Joint Engineering Research Center of MPTES in High Energy and Safety LIBs, Engineering Research Center of MTEES (Ministry of Education)
Key Lab. of ETESPG(GHEI), South China Normal University
Guangzhou, 510006 (P. R. China)
E-mail: chyf927821@163.com
          yqlan@m.scnu.edu.cn

Y.-J. Chen,[+] Prof. D. Yuan, Prof. G. Xu
State Key Laboratory of Structural Chemistry
Fujian Institute of Research on the Structure of Matter
Chinese Academy of Sciences (CAS), (P. R. China)
E-mail: gxu@fjirsm.ac.cn

M. Liu,[+] Dr. X. Huang,[+] Dr. L.-Z. Dong, Dr. M. Lu, Prof. Y. Chen, Prof. S.-L. Li, Prof. Y.-Q. Lan
Jiangsu Key Laboratory of Biofunctional Materials, School of Chemistry and Materials Science, Nanjing Normal University
Nanjing 210023 (P. R. China)
E-mail: yqlan@njnu.edu.cn

Y.-J. Chen,[+] Prof. G. Xu
University of Chinese Academy of Sciences (UCAS)
Beijing 100039 (P. R. China)

Prof. Y. Chen
Changzhou Institute of Innovation & Development Nanjing Normal University, Nanjing 210023 (P. R. China)

[+] These authors contributed equally to this work.

Introduction

Two-dimensional (2D) nanomaterials,[1] such as graphene, metal oxides, phosphorene, MXenes, and other 2D compounds, have been the subject of intensive research in the fields like energy storage, electrocatalysis, biochemical applications, and electronic equipment, etc.[2] Recently, 2D nanomaterials have also raised increasing interest as a new type of chemiresistive gas-sensing material due to their very desired performances at room temperature.[3] Their large surface-to-volume ratio offered a high number of sensing active-sites for high sensing sensitivity.[1b,3a,4] Their unique 2D geometry would directly expose the active sites to analyte molecules with a short mass transport pathway for fast response and recovery. The 2D structure also limited the carrier migration in the 2D plane, which facilitated the signal transduction and transfer.[3d,5] More importantly, their rich surface chemistry could immobilize additional functional motifs (e.g., organic molecules, metal or metal oxide nanoparticles, etc.),[6] which might further modulate the sensing properties. Nonetheless, the chemical modification still remained a daunting challenging for 2D nanomaterials due to their inert dangling-bond-free surfaces.[3d,7] Therefore, 2D materials with chemically modifiable surfaces are still highly sought after for developing high-performance room-temperature chemiresistive gas sensing.

Covalent organic frameworks (COFs), a kind of crystalline porous frameworks, are constructed by covalently connecting organic molecules.[8] They possess advantages like high stability, designable organic components, periodic pore structures and post-modifiable active sites, etc.[9] These features are rarely observed in traditional gas-sensing materials while very favored for gas sensing. However, most COFs were synthesized as irregular crystallites, which could not display all of the above-mentioned advantages and thus only two COF chemiresistive sensing materials have been reported and both displayed moderate sensing performances.[10] Given the advantages of 2D materials in gas sensing, fabricating COFs into 2D nanostructures was a viable strategy to make full use of their favorable features and improve their sensing performances. Moreover, COF 2D nanomaterials could be pre-designed with functional motifs for precise surface post-modification to overcome the above-mentioned issues in traditional 2D nanomaterials for sensing.[11] As far as we know, there have been limited reports on the fabrication of COFs into 2D nanomaterials, let alone their applications in gas sensing.[12] A new material design strategy that can rationally guide the preparation of

COF-based 2D nanomaterials at the molecular level is highly desired.

Porphyrin, which possesses a planar quadrangle geometry, is a popular organic component to construct COFs with 2D crystal structures.[13] Normally, its large π system results in strong inter-layer π–π interactions, which hampers the further exfoliation for 2D nanomaterials. In this work, density functional theory (DFT) calculations revealed that a porphyrin connected by linear bridge molecules would form planar layers with strong π–π stacking interaction as previously reported for COF-366.[14] While, a non-linear bridging component would distort the planar connection among the porphyrin rings to largely weaken the π–π stacking interaction among the COF layers. Inspired by these results, a non-linear 2,6-pyridinedicarboxaldehyde (PCBA) was selected to bridge 5,10,15,20-tetrakis(4-aminophenyl)porphyrin (TAPP) to form H₂-TPCOF. The connecting interaction between TAPP and PCBA drives the central triphenyl nucleus of PCBA to deviate from the same plane (torsion angles, 140° and 128°), resulting in obviously distorted 2D layers, a large interlayer distance and thus significantly reduced inter-layer packing interactions in H₂-TPCOF. A H₂-TPCOF 2D material with a thickness of ≈2 nm was obtained through a one-pot synthesis method. Different from the traditional 2D sensing materials, H₂-TPCOF had predesigned porphyrin rings as modifiable sites on its surface for post-metallization to flexibly modulate its sensing performance. Compared with H₂-TPCOF, the metal-lized M-TPCOF (M = Co and Cu) showed remarkably improved sensing performances, including ≈2 times higher sensitivity, ≈180 times lower limit-of-detection, ≈1.5 times faster response. Notably, Co-TPCOF exhibited a response as high as 2713 to 100 ppm NO_2, representing one of the most sensitive 2D materials.

Results and Discussion

H₂-TPCOF was firstly prepared by the condensation of TAPP and PCBA catalyzed by acetic acid under traditional solvothermal conditions and characterized (detail see Methods, Figure 1a and b). The crystal structure of H₂-TPCOF was elucidated by experimental powder X-ray diffraction (PXRD) measurements along with theoretical structural simulations by using the Materials Studio 7.0 software (Figure 1d, S1 and Table S1). The calculated PXRD pattern of eclipsed AA stacking of H₂-TPCOF was in accordance with the peak position and intensity of the experimental result (Figure S1). In detail, the intense peaks with 2θ at 4.30°, 8.58°, 11.31°, and 12.87° were assigned to (200), (400), (510), and (600) facets, respectively, and a broad diffraction peak at $2\theta = 21.96°$ was ascribed to the conjugation stacking of 2D layers (Figure 1d). With the introduction of the non-linear pyridine ligand, the plane structure of H₂-TPCOF was distorted owing to the non-linear connection between the aldehyde group and porphyrin node. Specifi-
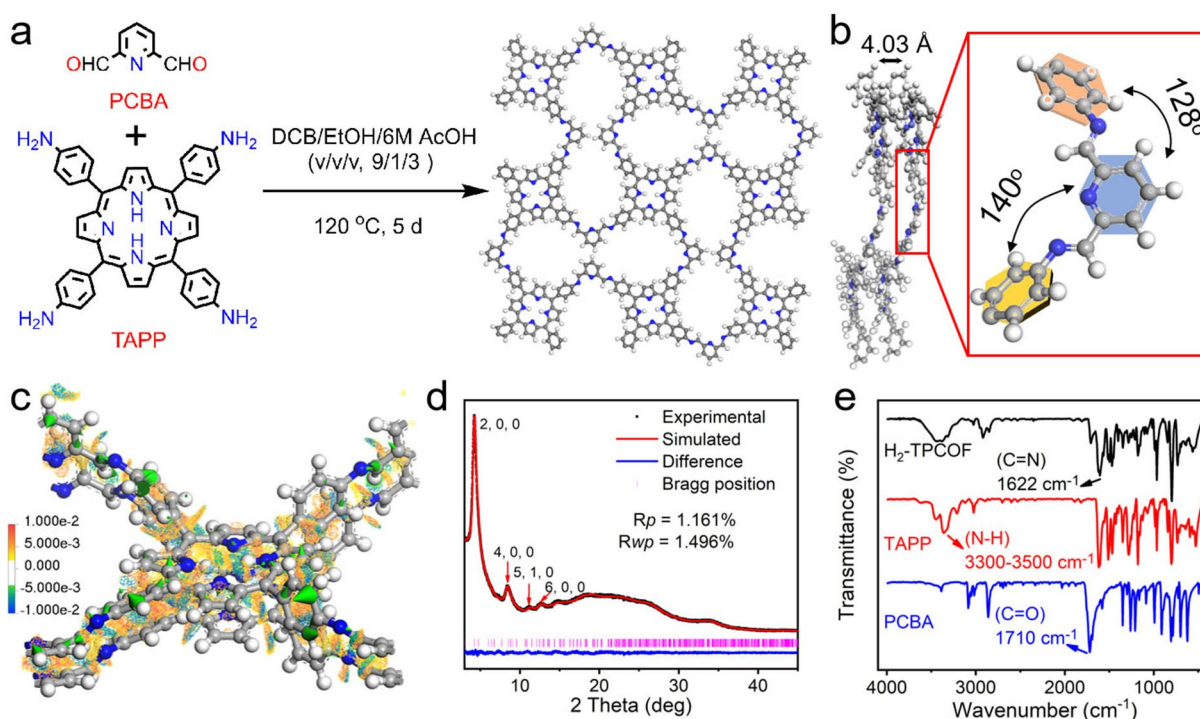

Figure 1. Structure and characterization of H₂-TPCOF. a) Schematic representation of the synthesis procedure and structure. b) Side view of the structure. c) Color-coded 3D scatterplot of sign(λ_2)ρ value at the region where values of reduced density gradient (RDG) are within [0.3, 0.6]. Green arrows manifest the forces exerted by the molecules in the underlying layer and more details of RDG and sign(λ_2)ρ can be found in the reported literature.[15] d) Experimental and simulated PXRD patterns. e) FT-IR spectra.

Angew. Chem. Int. Ed. **2022**, 61, e202115308 (2 of 7)

© 2022 Wiley-VCH GmbH

cally, the central triphenyl nucleus of PCBA was not on the same plane (torsion angles, 140° and 128°), resulting in the obvious distortion of the connected porphyrin rings to weaken the π–π stacking interaction (Figure 1b). To reveal it, DFT calculations were performed. COF-366,[14] a COF with a planar structure (the difference is PCBA replaced with p-benzaldehyde), was selected as the contrast sample (Figure S2). To show the regions and properties of non-covalent interactions (NCI) exited in COF-366 and H_2-TPCOF, we introduced NCI analysis,[15] which used the value of the reduced density gradient (RDG) to highlight the region of NCI, and used the product of the electron density and the second eigenvalue of the electron-density Hessian matrix [denoted as sign$(\lambda_2)\rho$] to show the properties of NCI. We observed that both structures possessed NCI between layers and had steric clashes (colored in red), and hydrogen bonds (colored in blue) as the NCI species (Figure 1c and Figure S3). In addition, the stacking energy for the interlayer interaction was calculated to be −6.98 eV for H_2-TPCOF, which was weaker than that of COF-366 (−7.47 eV). The more negative the energy value, the tighter the stack. These results indicated that H_2-TPCOF might more readily generate the 2D morphology than COF-366.

Besides, the as-synthesized H_2-TPCOF was further characterized by Fourier-transform infrared (FT-IR) and ^{13}C solid-state nuclear magnetic resonance (^{13}C NMR) spectroscopy, in which the imine linkages of the COF structure were confirmed. Concretely, the new absorption peak near 1622 cm^{-1} for the characteristic vibration of the C=N bond was observed in the FT-IR spectrum, which showed the existence of imine linkages of H_2-TPCOF. Besides, the almost disappearance of both the C=O vibration bond (1697 cm^{-1}) and the N–H stretching vibration bond (3300–3500 cm^{-1}) were probed (Figure 1e). Moreover, the formation of the C=N bond was evidenced by the appearance of signals at around 158 ppm in the ^{13}C NMR spectra, which clearly confirmed the structural integrity of H_2-TPCOF (Figure S4). For comparison, COF-366 was also synthesized and characterized as reported (Figure S5).[14]

Thereafter, the post-modification of M-TPCOF (M=Co and Cu) was prepared by direct metalation of H_2-TPCOF with transition metal acetates via a heat-assisted reflux method (detail see Methods). After post-metallization, no additional PXRD peaks emerged and the only observable change was the slightly decreased peak intensity, confirming the retention of the COF inert structures (Figure 2a). The FT-IR spectra of M-TPCOF (M=Co and Cu) coincide well with those of H_2-TPCOF, in which the C=N vibration bond was retained (Figure S6). The coordination of metal ions into H_2-TPCOF was further demonstrated by X-ray photoelectron spectroscopy (XPS) measurements (Figure 2b and S7–S11). Taking Co-TPCOF as an example, the observed Co $2p_{3/2}$ binding energy of 781.1 eV and $2p_{1/2}$ binding energy of 796.2 eV were assigned to Co^{II} (Figure S8), indicating the successful modification of Co ions into the structure.[13c,16] Impurities of other Co species (e.g., CoO and metallic Co) were not detected in Co-TPCOF (Figure 2b) and the Cu^{II} in Cu-TPCOF was also verified by XPS analysis (Figure S9). Meanwhile, compared with the N 1s XPS spectrum of H_2-
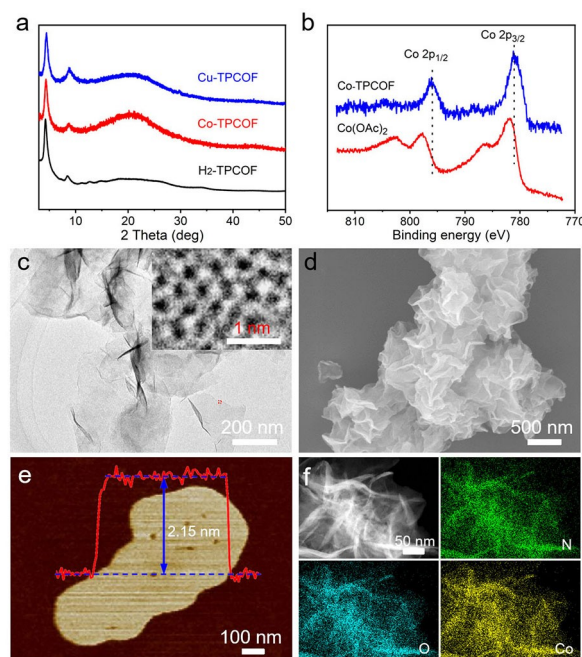

Figure 2. Structure and characterization of different samples. a) PXRD patterns of different samples. b) Co 2p XPS spectra of Co-TPCOF and Co(OAc)$_2$·4H$_2$O. c) TEM image of Co-TPCOF (inset high-resolution image is the red circled place in (c)). d) SEM image of Co-TPCOF. e) AFM image of Co-TPCOF (the red line is corresponding height profiles of the dispersed sheet). f) Elemental mapping images of Co-TPCOF.

TPCOF, an obvious upshift of N 1s peaks in Co-TPCOF was detected (Figure S10 and S11), which could also be attributed to the coordination of nitrogen atoms to Co ions.[16,17]

Transmission electron microscopy (TEM) and scanning electron microscopy (SEM) were further applied to characterize the morphologies of the samples. COF-366 was synthesized and it only possessed a large and irregular particle morphology, which was quite different from H_2-TPCOF (detail see Methods, Figure S12 and S13). As for H_2-TPCOF and M-TPCOF, the TEM tests of them showed ultrathin nanosheets (size of ≈500 nm) (Figure 2c and S13). Besides, high-resolution TEM images displayed that the periodic pore networks were clearly visualized for Co-TPCOF (inset image of Figure 2c). The SEM image of Co-TPCOF exhibited dispersed flakes with a wrinkled surface (Figure 2d), complying with the results of TEM measurement. In addition, atomic force microscopy (AFM) has been conducted and the average thickness of Co-TPCOF was determined to be 2.15 nm (Figure 2e). According to the optimized calculation of the COF model, the obtained nanosheets were composed of about five monolayers (the distance between adjacent monolayers was ≈4.03 Å) (Figure 1b and 2e). The morphology results are in accord with the hypothesis mentioned above that the lower interlayer interaction in the structure would be beneficial for the generation of 2D morphology. In addition, the obtained ultra-thin nanosheets with thickness on the atomic level were extremely important for the fully accessible and

exposed active sites, which were favorable for the gas diffusion and sensing applications. Moreover, EDS mapping images revealed that C, N, O and Co were uniformly distributed in Co-TPCOF (Figure 2f). The total Co and Cu content in M-TPCOF were detected to be 4.93 wt% and 4.78 wt% by inductively coupled plasma optical emission spectrometer (ICP-OES) analyses, respectively (Table S2). For comparison, Cu-TPCOF showed a similar morphology to that of Co-TPCOF as proved by SEM, TEM and EDS mapping tests (Figure S14 and S15).

It has been reported that COF-366 had a Brunauer–Emmett–Teller (BET) surface area (S_{BET}) of $\approx 1300\ m^2\,g^{-1}$.[14] The accessible porosities of the as-obtained materials were studied by N_2 sorption tests at 77 K. The S_{BET} of H_2-TPCOF was 757 $m^2\,g^{-1}$. After post-metallization, M-TPCOF (M = Co and Cu) had a decreased S_{BET} and they were 445 $m^2\,g^{-1}$ for Co and 329 $m^2\,g^{-1}$ for Cu, respectively (Table S3 and Figure S16–S18). Thermogravimetric (TGA) analysis showed no obvious change of weight loss for these samples when the temperature increased to 300 °C, implying the high thermal stability (Figure S19).

To evaluate the sensing performances, H_2-TPCOF, M-TPCOF and COF-366 were deposited on interdigital electrodes by a drop-coating method and the current signals of the devices in different gaseous analytes were recorded (detail see Methods). To ensure the accuracy of the test results, two devices were prepared in parallel for the same sample. All tests were performed at room temperature.

The relative current variation before and after exposure to the analyte was defined as device responsivity. To 100 ppm NO_2, 5,10,15,20-tetraphenylporphyrin (TPP) and COF-366 (S_{BET}, $\approx 1300\ m^2\,g^{-1}$) presented response values of 5.34 and 92.3, respectively, which were significantly lower than that of H_2-TPCOF (response, 1382 and S_{BET}, 757 $m^2\,g^{-1}$) (Figure S20–S22). Similar results were obtained for M-TPCOF (M = Co and Cu), which possessed a much lower S_{BET} value, while it showed a higher sensing response (2713 for Co, 2056 for Cu) to 100 ppm NO_2 in both of the samples (Figure 3a and S23). These results suggested the S_{BET} value and response results of these materials were not positively correlated and the exposed metal active sites on the outer surface might facilitate the interaction with NO_2 and effectively optimize the sensitivity. Interestingly, Co-TPCOF also exhibited high response/recovery performance in a wide range of NO_2 concentrations (Figure 3a). The low coefficient of variation (CV = 9.4%) toward 10 ppm NO_2 was detected over four continuous cycles, indicating excellent repeatability (Figure 3a). Notably, the response-concentration log-log plots of Co-TPCOF exhibited good linearity ($R^2 = 0.99$) and the calculated LOD was 6.8 ppb (Figure 3b), which was the lowest among reported COFs[10] and superior to most of NO_2 sensing materials (Table S4).[3d,18]

The response time (t_{res}: defined as the time achieved for increasing the current to 90% of the maximum signal) of samples upon exposure to 10 ppm NO_2 have been evaluated. The t_{res} (12.6 min) of COF-366 was longer than that of H_2-TPCOF (8.7 min) (Figure S21 and S22), which might be attributed to the fast adsorption of NO_2 in the ultra-thin
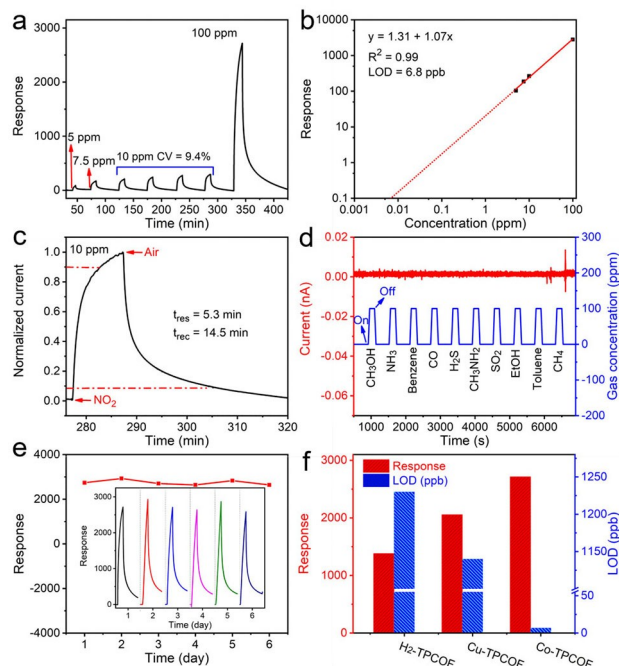

Figure 3. Gas-sensing performances of the devices at room temperature. a) Dynamic response curves of Co-TPCOF toward 5–100 ppm NO_2. b) Linear relationship of response vs. NO_2 concentration of Co-TPCOF. c) Normalized response–recovery time curves for Co-TPCOF to 10 ppm NO_2. d) Sensing current of Co-TPCOF to 10 types of interfering gases (100 ppm). e) Stability of Co-TPCOF to 100 ppm NO_2 within 6 days (inset curves are the real-time measurement). f) Response and LOD column of different samples.

nanosheet of H_2-TPCOF (≈ 2 nm). Besides, the t_{res} of Co-TPCOF has been tested to be 5.3 min (Figure 3c). The lower t_{res} of Co-TPCOF than that of H_2-TPCOF might be ascribed to the fully exposed Co active sites in the ultra-thin nanosheets morphology that can facilitate the interaction with NO_2.

Selectivity was a vital parameter for the function evaluation of sensing materials.[19] The current data of Co-TPCOF upon exposure to 10 types of other interfering gases at the concentration of 100 ppm for 3 min are shown in Figure 3d. Notably, no apparent change of current was observed toward 10 commonly cross-sensitive gases involving SO_2,[20] a representative interference gas for NO_2, implying that Co-TPCOF possessed excellent selectivity. As far as we know, such unusual specific selectivity has rarely been reported for NO_2 sensing materials.[3a,4,10b]

Moreover, the long-term stability has been tested based on Co-TPCOF. The results revealed that Co-TPCOF had good long-term stability and its response showed minor changes during 6 days, possibly due to the stable covalent bonds in the COF structure (Figure 3e). In addition, a PXRD test showed the remaining inert structure of Co-TPCOF after the long-term test (Figure S24), indicating its high stability when exposed to NO_2.

To understand the excellent performance of Co-TPCOF, DFT calculations were performed. Firstly, we calculated the

adsorption energy (E_{ad}), and the nearest atomic distance between 11 gas molecules (e.g., NO_2, NH_3, SO_2, and CH_3NH_2, etc.) and the Co-porphyrin portion of Co-TPCOF. The top view and side view of the optimized gases adsorption geometries mode on the Co-porphyrin portion of the COF skeleton are shown in Figure S25. For NO_2, the N atom points to the basic unit of Co-TPCOF and the nearest distance between NO_2 and Co-TPCOF is 1.87 Å (Table S5), which is smaller than the reported calculated adsorption value of the Co–N bond length (2.07 Å).[21] Moreover, the adsorption energies for the measured analytes were negative, which indicated the spontaneity of the adsorption process and the stability of the various adsorbed gases on the sensing material surface. It was worth noting that NO_2 had the largest adsorption energy of −1.52 eV on the Co-porphyrin portion of Co-TPCOF, which is much higher than other gas molecules and supported the high selectivity of Co-TPCOF towards NO_2 (Figure 4a and Table S5).

We also calculated the E_{ad} and nearest atomic distance between 11 gas molecules (e.g., NO_2, NH_3, SO_2, and CH_3NH_2 etc.) and the Co-pyridine portion of Co-TPCOF (Figure S26 and Table S6). It could be seen that the gas adsorption on the Co-pyridine center was generally weaker than that on the Co-porphyrin, especially for NO_2. For NO_2, the E_{ad} on Co-pyridine center (−0.22 eV) was much lower than that on the Co-porphyrin center (−1.52 eV). Besides, the nearest distance between NO_2 and the Co-pyridine center was 3.23 Å, which was also much longer than on the Co-porphyrin center (1.87 Å). The results suggested the dominant role of the Co-porphyrin in the interaction with NO_2 and the Co sites modified at the pyridine had a minor effect on the interaction. Furthermore, DFT calculations revealed that the Co-porphyrin portion gives a much higher E_{ad} (−1.52 eV) to NO_2 than H_2-TPCOF (−0.27 eV) and Cu-TPCOF (−0.47 eV) (Figure S27 and Table S7), which supported its highest sensitivity of all COF 2D materials.

The adsorption of NO_2 on Co-TPCOF was further demonstrated by in situ diffuse reflectance infrared Fourier transform (DRIFT) spectroscopy (Figure 4b). The gradually strengthened signals in the region of 2500 to 1000 cm^{-1} for the Co-TPCOF revealed the adsorption of NO_2 and the formation of adsorbed intermediate nitrite species. The broad peak at 1500–1290 cm^{-1} represented the N=O stretching vibration of the monodentate nitrite or the asymmetric stretching NO_2 vibration of nitro group.[22] Among them, the peak at 1398–1353 cm^{-1} belonged to Co-NO_2 nitro compounds, proving that Co was the active site of NO_2 induction.[23] Therefore, the NO_2^- species would be produced by the one-electron reduction of adsorbed NO_2 during the NO_2 adsorption process. The wide high-intense peak observed at 2310–2230 cm^{-1} might be due to the N=O vibrations in nitrosonium NO^+.[22b] In addition, the peaks appearing at 1548 cm^{-1} and 1205 cm^{-1} were ascribed to stretching vibrations of N–O bonds in monodentate nitrite species.[22a]

According to the above discussion, a possible selective sensing process of M-TPCOF is suggested as follows (Figure 4c): taking Co-TPCOF for instance, when the surface of Co-TPCOF was exposed to NO_2, the NO_2 could quickly adsorb on it. Simultaneously, NO_2 as the strong electron acceptor received electrons from the Co active sites through the strong interaction (e.g., chemisorption or coordination interaction, etc.) to form nitrite species (e.g., NO^+ and NO_2^-, etc.), resulting in the dramatic increase of hole concentration for the p-type Co-TPCOF and leading to the change in the conductivity.[20] Once NO_2 was removed from the surface of Co-TPCOF, the trapped electrons of the formed NO_2^- released back to Co-TPCOF and desorb, causing the current recovery of the sensor. The specific sensing nature of M-TPCOF might be due to the much stronger interaction to NO_2 than other gases.

Conclusion

In conclusion, to overcome the chemically inert surface of traditional 2D materials for chemiresistive gas sensing, we have synthesized a series of COF-based 2D nanomaterials. The specifically designed H_2-TPCOF, assembled from a non-linear bridging ligand and a porphyrin component, had largely reduced interlayer stress and enabled a direct synthesis of ultrathin nanosheets. The predesigned porphyrin rings act as modifiable sites on its surface for post-metallization to flexibly modulate its sensing performance. After post-metallization, the metallized M-TPCOF (M = Co and Cu) showed remarkably improved sensing performances. Among them, Co-TPCOF exhibited highly specific sensing toward NO_2 with one of the highest sensitivities among all reported 2D materials and COF materials, an ultra-low LOD of 6.8 ppb and fast response speed. Notably, the sensing mechanism has been intensively studied by DFT calculations, which revealed the vital role of the Co-porphyrin center. This work should provide a new pathway for designing 2D sensing materials with a rich surface chemistry.
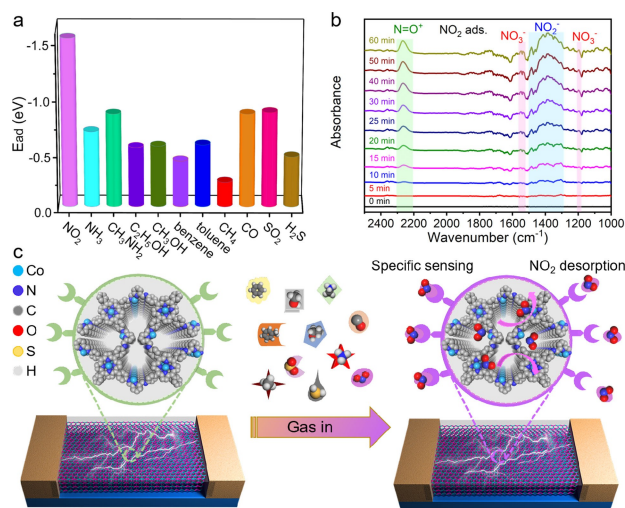

Figure 4. DFT calculations and in-situ DRIFT tests of Co-TPCOF. a) 3D histogram of adsorption energy of Co-TPCOF for different gases. b) In situ DRIFT spectra of Co-TPCOF during NO_2 adsorption. c) Schematic illustration of specific sensing of Co-TPCOF for NO_2.

Acknowledgements

Conflict of Interest

The authors declare no conflict of interest.

Data Availability Statement

The data that support the findings of this study are available from the corresponding author upon reasonable request.

Keywords: Covalent Organic Frameworks · Gas Sensors · Nanosheets · Porphyrin · Post-Metallization

[1] a) Y. Chen, Z. Fan, Z. Zhang, W. Niu, C. Li, N. Yang, B. Chen, H. Zhang, *Chem. Rev.* **2018**, *118*, 6409–6455; b) C. Tan, X. Cao, X.-J. Wu, Q. He, J. Yang, X. Zhang, J. Chen, W. Zhao, S. Han, G.-H. Nam, M. Sindoro, H. Zhang, *Chem. Rev.* **2017**, *117*, 6225–6331.

[2] a) Y. Pang, C. Su, G. Jia, L. Xu, Z. Shao, *Chem. Soc. Rev.* **2021**, *50*, 12744–12787; b) A. Molle, C. Grazianetti, L. Tao, D. Taneja, M. H. Alam, D. Akinwande, *Chem. Soc. Rev.* **2018**, *47*, 6370–6387; c) X. Yin, C. S. Tang, Y. Zheng, J. Gao, J. Wu, H. Zhang, M. Chhowalla, W. Chen, A. T. S. Wee, *Chem. Soc. Rev.* **2021**, *50*, 10087–10115; d) L. Li, S. Zhang, Y. Lu, J. Zhang, X. Zhang, R. Wang, J. Huang, *Adv. Mater.* **2021**, *33*, 2104120; e) C. Cao, D.-D. Ma, J.-F. Gu, X. Xie, G. Zeng, X. Li, S.-G. Han, Q.-L. Zhu, X.-T. Wu, Q. Xu, *Angew. Chem. Int. Ed.* **2020**, *59*, 15014–15020; *Angew. Chem.* **2020**, *132*, 15124–15130.

[3] a) N. Rohaizad, C. C. Mayorga-Martinez, M. Fojtů, N. M. Latiff, M. Pumera, *Chem. Soc. Rev.* **2021**, *50*, 619–657; b) S. Mao, J. Chang, H. Pu, G. Lu, Q. He, H. Zhang, J. Chen, *Chem. Soc. Rev.* **2017**, *46*, 6872–6904; c) D. H. Ho, Y. Y. Choi, S. B. Jo, J.-M. Myoung, J. H. Cho, *Adv. Mater.* **2021**, *33*, 2005846; d) Z. Meng, R. M. Stolz, L. Mendecki, K. A. Mirica, *Chem. Rev.* **2019**, *119*, 478–598.

[4] a) J. Zhang, X. Liu, G. Neri, N. Pinna, *Adv. Mater.* **2016**, *28*, 795–831; b) T. Liang, Z. Dai, Y. Liu, X. Zhang, H. Zeng, *Sci. Bull.* **2021**, *66*, 2471–2478.

[5] M. Zeng, Y. Xiao, J. Liu, K. Yang, L. Fu, *Chem. Rev.* **2018**, *118*, 6236–6296.

[6] a) S. Shui-Fa, Q. Kai-Tao, C. Jian-Ping, W. Meng-Yang, *Chin. J. Struct. Chem.* **2019**, *38*, 1743–1751; b) A. Hirsch, F. Hauke, *Angew. Chem. Int. Ed.* **2018**, *57*, 4338–4354; *Angew. Chem.* **2018**, *130*, 4421–4437; c) V. Georgakilas, M. Otyepka, A. B. Bourlinos, V. Chandra, N. Kim, K. C. Kemp, P. Hobza, R. Zboril, K. S. Kim, *Chem. Rev.* **2012**, *112*, 6156–6214; d) Z. Li, S. L. Wong, *Mater. Sci. Eng. C* **2017**, *70*, 1095–1106; e) G. C. Guo, Y. G. Yao, K. C. Wu, L. Wu, J. S. Huang, *Prog. Chem.* **2001**, *13*, 151–155.

[7] a) C. Tan, H. Zhang, *Chem. Soc. Rev.* **2015**, *44*, 2713–2731; b) Z. Lin, A. McCreary, N. Briggs, S. Subramanian, K. Zhang, Y. Sun, X. Li, N. J. Borys, H. Yuan, S. K. Fullerton-Shirey, A. Chernikov, H. Zhao, S. McDonnell, A. M. Lindenberg, K. Xiao, B. J. LeRoy, M. Drndić, J. C. M. Hwang, J. Park, M. Chhowalla, R. E. Schaak, A. Javey, M. C. Hersam, J. Robinson, M. Terrones, *2D Mater.* **2016**, *3*, 042001.

[8] a) C. S. Diercks, O. M. Yaghi, *Science* **2017**, *355*, eaal1585; b) H. S. Sasmal, S. Bag, B. Chandra, P. Majumder, H. Kuiry, S. Karak, S. Sen Gupta, R. Banerjee, *J. Am. Chem. Soc.* **2021**, *143*, 8426–8436.

[9] a) K. Geng, T. He, R. Liu, S. Dalapati, K. T. Tan, Z. Li, S. Tao, Y. Gong, Q. Jiang, D. Jiang, *Chem. Rev.* **2020**, *120*, 8814–8933; b) R.-R. Liang, S.-Y. Jiang, R.-H. A, X. Zhao, *Chem. Soc. Rev.* **2020**, *49*, 3920–3951; c) X. Han, C. Yuan, B. Hou, L. Liu, H. Li, Y. Liu, Y. Cui, *Chem. Soc. Rev.* **2020**, *49*, 6248–6272; d) K. Dey, S. Kunjattu H, A. M. Chahande, R. Banerjee, *Angew. Chem. Int. Ed.* **2020**, *59*, 1161–1165; *Angew. Chem.* **2020**, *132*, 1177–1181.

[10] a) Z. Meng, R. M. Stolz, K. A. Mirica, *J. Am. Chem. Soc.* **2019**, *141*, 11929–11937; b) Y. Yue, P. Cai, X. Xu, H. Li, H. Chen, H.-C. Zhou, N. Huang, *Angew. Chem. Int. Ed.* **2021**, *60*, 10806–10813; *Angew. Chem.* **2021**, *133*, 10901–10908.

[11] a) S. Y. Choi, Y. Kim, H.-S. Chung, A. R. Kim, J.-D. Kwon, J. Park, Y. L. Kim, S.-H. Kwon, M. G. Hahm, B. Cho, *ACS Appl. Mater. Interfaces* **2017**, *9*, 3817–3823; b) Y. Wen, G.-E. Wang, X. Jiang, X. Ye, W. Li, G. Xu, *Angew. Chem. Int. Ed.* **2021**, *60*, 19710–19714; *Angew. Chem.* **2021**, *133*, 19862–19866; c) J. Li, X. Jing, Q. Li, S. Li, X. Gao, X. Feng, B. Wang, *Chem. Soc. Rev.* **2020**, *49*, 3565–3604.

[12] X. Liu, D. Huang, C. Lai, G. Zeng, L. Qin, H. Wang, H. Yi, B. Li, S. Liu, M. Zhang, R. Deng, Y. Fu, L. Li, W. Xue, S. Chen, *Chem. Soc. Rev.* **2019**, *48*, 5266–5302.

[13] a) J.-L. Shi, R. Chen, H. Hao, C. Wang, X. Lang, *Angew. Chem. Int. Ed.* **2020**, *59*, 9088–9093; *Angew. Chem.* **2020**, *132*, 9173–9178; b) E. Tavakoli, A. Kakekhani, S. Kaviani, P. Tan, M. M. Ghaleni, M. A. Zaeem, A. M. Rappe, S. Nejati, *J. Am. Chem. Soc.* **2019**, *141*, 19560–19564; c) M. Lu, J. Liu, Q. Li, M. Zhang, M. Liu, J.-L. Wang, D.-Q. Yuan, Y.-Q. Lan, *Angew. Chem. Int. Ed.* **2019**, *58*, 12392–12397; *Angew. Chem.* **2019**, *131*, 12522–12527; d) R. Chen, Y. Wang, Y. Ma, A. Mal, X.-Y. Gao, L. Gao, L. Qiao, X.-B. Li, L.-Z. Wu, C. Wang, *Nat. Commun.* **2021**, *12*, 1354.

[14] S. Lin, C. S. Diercks, Y.-B. Zhang, N. Kornienko, E. M. Nichols, Y. Zhao, A. R. Paris, D. Kim, P. Yang, O. M. Yaghi, C. J. Chang, *Science* **2015**, *349*, 1208–1213.

[15] J. Contreras-García, E. R. Johnson, S. Keinan, R. Chaudret, J.-P. Piquemal, D. N. Beratan, W. Yang, *J. Chem. Theory Comput.* **2011**, *7*, 625–632.

[16] H. B. Aiyappa, J. Thote, D. B. Shinde, R. Banerjee, S. Kurungot, *Chem. Mater.* **2016**, *28*, 4375–4379.

[17] a) A. M. Beiler, D. Khusnutdinova, B. L. Wadsworth, G. F. Moore, *Inorg. Chem.* **2017**, *56*, 12178–12185; b) X. Ma, C. Pang, S. Li, Y. Xiong, J. Li, J. Luo, Y. Yang, *Biosens. Bioelectron.* **2019**, *146*, 111734.

[18] a) K. Yang, W. Yuan, Z. Hua, Y. Tang, F. Yin, D. Xia, *ACS Appl. Mater. Interfaces* **2020**, *12*, 3919–3927; b) W. Yuan, G. Shi, *J. Mater. Chem. A* **2013**, *1*, 10078–10091; c) H. Peng, F. Li, Z. Hua, K. Yang, F. Yin, W. Yuan, *Sens. Actuators B* **2018**, *275*, 78–85; d) X. Liu, T. Ma, N. Pinna, J. Zhang, *Adv. Funct. Mater.* **2017**, *27*, 1702168.

[19] M.-S. Yao, W.-X. Tang, G.-E. Wang, B. Nath, G. Xu, *Adv. Mater.* **2016**, *28*, 5229–5234.

[20] H. Jiang, L. Cao, Y. Li, W. Li, X. Ye, W. Deng, X. Jiang, G. Wang, G. Xu, *Chem. Commun.* **2020**, *56*, 5366–5369.

Angew. Chem. Int. Ed. **2022**, *61*, e202115308 (6 of 7)

© 2022 Wiley-VCH GmbH

[21] S. Shang, C. Yang, C. Wang, J. Qin, Y. Li, Q. Gu, J. Shang, *Angew. Chem. Int. Ed.* **2020**, *59*, 19680–19683; *Angew. Chem.* **2020**, *132*, 19848–19851.

[22] a) L. Yang, A. Marikutsa, M. Rumyantseva, E. Konstantinova, N. Khmelevsky, A. Gaskov, *Sensors* **2019**, *19*, 3405; b) K. I. Hadjiivanov, *Catal. Rev.* **2000**, *42*, 71–144.

[23] a) G. Gao, J.-W. Shi, Z. Fan, C. Gao, C. Niu, *Chem. Eng. J.* **2017**, *325*, 91–100; b) L. Zhang, L. Shi, L. Huang, J. Zhang, R. Gao, D. Zhang, *ACS Catal.* **2014**, *4*, 1753–1763.